Spontaneous emission from dipole-forbidden transitions in semiconductor quantum dots

Michele Cotrufo* and Andrea Fiore
COBRA Research Institute, Eindhoven University of Technology, 5600 MB Eindhoven, The Netherlands
(Received 20 December 2014; revised manuscript received 13 July 2015; published 1 September 2015)

We theoretically investigate the multipolar effects on the dipole-forbidden transitions of a semiconductor quantum dot. An approximated expression for the decay rate of these transitions is derived. Unlike the general theory of the spontaneous emission beyond the dipole approximation, the distinct roles of the emitter and the vacuum electric field in the transition rate are here clearly recognizable and can be separately optimized. We illustrate the potential of this formalism by calculating the spontaneous emission decay rate of an InAs/GaAs quantum dot embedded into two realistic nanostructures—an L3 photonic crystal cavity and a plasmonic dimer antenna. The obtained results show that, although the two structures provide an enhancement of the same order of magnitude, the plasmonic antenna constitutes a more promising candidate for the experimental observation of the dipole-forbidden transitions of a quantum dot.

DOI: 10.1103/PhysRevB.92.125302 PACS number(s): 78.67.Hc

I. INTRODUCTION

Semiconductor quantum dots (QDs) have become a subject of intensive research [1] in the recent years for both fundamental and applicative purposes. The emission spectrum of these heterostructures shows an atomiclike behavior, with sharp lines in correspondence with the optically active transitions between the discrete energy levels. The great advantage of these emitters as compared to atoms or molecules is the possibility of tuning their optical properties, either in a static way by engineering the size, shape, and chemical composition, or in a dynamic way by, e.g., varying the strain [2], controlling the temperature [3], and applying an external electric [4] or magnetic [5] field. These properties, together with the compatibility with the existing semiconductor technology, make the QDs promising light sources for novel devices, such as QD lasers [6] and single photon sources.

When describing the light-matter interaction, one usually assumes that the emitter can be considered pointlike with respect to the spatial variation of the electromagnetic field. This approach constitutes the well-known dipole approximation, which is an excellent approximation for atoms emitting in the visible part of the spectrum, since their dimensions are several orders of magnitude smaller than the optical wavelength. This assumption greatly simplifies the theoretical framework of the spontaneous emission, and provides simple selection rules to identify the optically active transitions.

Despite their atomiclike spectrum, QDs are inherently different from atoms because of their mesoscopic size: the excitation is distributed over the entire volume of the QD, which usually includes up to 10^5 atoms. The large extent of the exciton wave function makes the validity of the dipole approximation questionable. In a bulk material, the vacuum electromagnetic field can be described by plane waves and the typical criterion for the validity of the dipole approximation is that $|\mathbf{k}|L \ll 1$, where $|\mathbf{k}| = 2\pi n/\lambda$ is the modulus of the light wave vector, λ is the optical wavelength, n is the refractive index of the material, and L is the spatial extent of the wave function of the emitter. The value of $|\mathbf{k}|$ is increased in high-refractive-index semiconductors such that, for the typical dimensions of a semiconductor QD, the value of $|\mathbf{k}|L$ is not necessarily negligible, even in the visible or near-IR range. As an example, for an InAs/GaAs QD emitting at a wavelength of 1300 nm and with a characteristic dimension of $L = 10$ nm, $|\mathbf{k}|L \simeq 0.16$. Moreover, in artificial photonic nanostructures the aforementioned criterion is not applicable anymore, since the electromagnetic field at a certain frequency can feature spatial variations corresponding to $|\mathbf{k}|$ values larger than the plane wave in a bulk material. These situations can introduce non-negligible corrections, as recently demonstrated in an experimental work [7] where the decay rate of QDs in close proximity to a metallic mirror has been shown to differ from the dipole approximation predictions. As the combination of QDs with nanophotonic cavities is a key ingredient for the realization of efficient single-photon sources [1] and nanolasers [6], it is essential to understand the radiative properties of these structures beyond the dipole approximation.

In the past years, there have been several proposals [8–11] to include multipolar effects into the theory of the spontaneous emission of a QD. In a recent paper by Stobbe *et al.* [12] it has been shown how to calculate the decay rate of a semiconductor QD when the electric field along the emitter wave functions cannot be assumed constant. The authors showed that when this theory is applied to the radiative transitions of a QD placed in a strongly inhomogeneous field, substantial deviations from the dipole approximation predictions are obtained.

Another interesting effect can be investigated with the aid of this theory. When describing the QD states within the envelope-function formalism [13], the selection rules dictate that certain excitonic transitions, usually referred as *dipole-forbidden*, cannot occur radiatively. The reason for this is that, having assumed the electromagnetic field constant over the QD, the matrix element of the transition is given by the product of the overlap integral of the electron and the hole envelope functions and the Bloch matrix element. The former depends on the exciton involved in the transition

*m.cotrufo@tue.nl

while the latter depends, in a first approximation [13], only on the materials used and not on the QD structural parameters. The envelope functions feature different parities with respect to the QD center, which affects the value of the overlap integral. Excitonic states characterized by electron and hole envelope functions with different parities will have a small value of the overlap integral (zero if the QD is symmetric) and therefore a negligible radiative decay rate (compared to the one of the optically active transitions, usually referred as *dipole-allowed*). However, when the spatial variation of the field is not negligible anymore, the matrix element of the transition can be sensitively altered.

Besides this fundamental interest, dipole-forbidden transitions can play a role in the spectral properties and radiative dynamics of QDs embedded in nanophotonic devices, which makes their investigation relevant for their applications. The purpose of this paper is to theoretically investigate these effects, firstly by deriving a simplified formula for the decay rate of the dipole-forbidden transitions and identifying the figures of merit for its enhancement, and secondly by applying this formalism to realistic nanostructures, in order to evaluate the magnitude of these effects.

The paper is organized as follows. In Sec. II A, the theory to calculate the spontaneous emission from QDs beyond the dipole approximation is briefly summarized. In Sec. II B, we apply this theory to the particular case of the dipole-forbidden transitions, and we derive a simpler formula, which clarifies the figure of merit for the spontaneous emission decay rate. In Sec. III, we apply our formalism to the case of a QD interacting with two possible photonic nanostructures, an L3 photonic crystal cavity (Sec. III B), and a plasmonic antenna (Sec. III C). In Sec. III D, we show how the enhancement of the decay rate obtained in these two cases, although of the same order of magnitude, is due to two different physical phenomena. Finally, the conclusions are drawn in Sec. IV.

II. THEORY

A. Spontaneous emission from semiconductor quantum dots beyond the dipole approximation

The quantum state of an exciton in a semiconductor QD can be described in a first approximation through a two-band model. Although the upper valence bands in III-V semiconductors are degenerate in bulk materials, the presence of the strain and confinement in a QD lifts the degeneracy; the electron-hole interactions can therefore be restricted to the conduction band and the heavy-hole valence band. By approximating the periodic part of the Bloch function with its value at $\mathbf{k} = 0$, the wave function of the exciton can be written as

$$\Psi(\mathbf{r}_e,\mathbf{r}_h) = \chi(\mathbf{r}_e,\mathbf{r}_h) u_{c,0}(\mathbf{r}_e) u_{v,0}(\mathbf{r}_h), \tag{1}$$

where $\mathbf{r}_e$ ($\mathbf{r}_h$) is the electron (hole) position, $u_{c,0}$ ($u_{v,0}$) is the periodic part of the conduction (valence) band Bloch function at $\mathbf{k}_e = \mathbf{k}_h = 0$ and $\chi(\mathbf{r}_e,\mathbf{r}_h)$ is the so-called envelope function. This function is obtained as a solution of an effective-mass Hamiltonian,

$$H(\mathbf{r}_e,\mathbf{r}_h) = \frac{\hat{\mathbf{p}}_e^2}{2m_e^*} + \frac{\hat{\mathbf{p}}_h^2}{2m_h^*} + V_e(\mathbf{r}_e) + V_h(\mathbf{r}_h) + H_C(\mathbf{r}_e,\mathbf{r}_h), \tag{2}$$

which contains the confinement potential for the electrons (V_e) and the holes (V_h) and the mutual Coulomb interaction $H_C(\mathbf{r}_e,\mathbf{r}_h)$. In the *strong-confinement limit*, the Coulomb energy is much smaller than the energy levels spacing induced by the quantum confinement and can be neglected. Therefore, in a first approximation, the effective-mass equation is separable into the electron and hole coordinates and the solution is given as a product of the single-particle envelope functions, $\chi(\mathbf{r}_e,\mathbf{r}_h) = \chi_e(\mathbf{r}_e) \cdot \chi_h(\mathbf{r}_h)$.

The spontaneous emission decay rate is not an intrinsic property of an emitter but it depends on the vacuum electromagnetic field in which the emitter is embedded. In the dipole approximation theory, this dependence is included through the concept of the *local density of states* (LDOS) [14], which gives, for each spatial point, the density of the photonic states available for the exciton to decay into. The LDOS in a certain point is proportional to the modulus square of the vacuum electric field in that point. The knowledge of the electric field in the center of the QD is therefore sufficient to calculate the spontaneous decay rate. Instead, as shown by Stobbe *et al.* [12], the mesoscopic nature of the QD requires the knowledge of the electromagnetic Green tensor, $G(\mathbf{r},\mathbf{r}',\omega)$, which gives, up to a constant factor, the electric field in a position $\mathbf{r}$ generated by a dipolar source placed in $\mathbf{r}'$ and emitting with frequency ω.

Once the emitter's and electromagnetic field's properties are known (through the exciton wave function and the Green tensor, respectively) the decay rate of a QD beyond the dipole approximation (Γ_{BDA}) can be calculated as [12]

$$\Gamma_{\mathrm{BDA}}(\omega) = \frac{2e^2}{\hbar\epsilon_0 m_0^2 c^2} |\mathbf{p}_{\mathrm{cv}}|^2 \int d^3\mathbf{r} \times \int d^3\mathbf{r}' \chi(\mathbf{r},\mathbf{r}) \chi^*(\mathbf{r}',\mathbf{r}') \mathrm{Im}[G_{pp}(\mathbf{r},\mathbf{r}',\omega)], \tag{3}$$

where e is the elementary charge, $\hbar$ is the reduced Planck constant, ϵ_0 is the vacuum permittivity, m_0 is the free electron mass, and c is the speed of light in vacuum. The vector $\mathbf{p}_{\mathrm{cv}} = \langle u_{c,0} | \hat{\mathbf{p}} | u_{v,0} \rangle$, where $\hat{\mathbf{p}}$ is the momentum operator, is the Bloch matrix element and it is a parameter of the material used. Its direction affects the coupling of the exciton to the different polarizations of the field. For the transitions between the lowest energy states in typical self-assembled QDs, this vector usually lies in the plane of growth [15]. The diagonal component G_{pp} of the Green tensor is used, where p is the direction parallel to $\mathbf{p}_{\mathrm{cv}}$.

As already pointed out by the authors of the theory in Ref. [12], Eq. (3) contains the dipole approximation as a particular case: when the field is slowly varying over the function $\chi(\mathbf{r}_e,\mathbf{r}_h)$, the Green tensor can be calculated in the center $\mathbf{r}_0$ of the emitter and taken out of the integral,

$$\Gamma_0(\omega) = \frac{2e^2}{\hbar\epsilon_0 m_0^2 c^2} |\mathbf{p}_{\mathrm{cv}}|^2 \mathrm{Im}[G_{pp}(\mathbf{r}_0,\mathbf{r}_0,\omega)] \left| \int d^3\mathbf{r} \chi(\mathbf{r},\mathbf{r}) \right|^2. \tag{4}$$

Here and in what follows, Γ_0 indicates the decay rate calculated within the dipole approximation. The decay rate is given by the product of a quantity that depends on the field (and which can be shown to be proportional to the LDOS) [14] and a quantity that depends on the exciton state and is proportional

to the oscillator's strength of the transition. This separation of the degrees of freedom is the main result of the dipole approximation theory. The decay rate is different from zero only if the overlap integral of the electron and hole envelope functions does not vanish (except for the particular case in which the emitter is placed in a node of the electromagnetic field, which makes the Green tensor null).

On the other hand, Eq. (3) shows a much more complicated behavior, since the photonic and excitonic degrees of freedom are not directly separable. An excitonic transition for which the overlap integral of the envelope functions is zero (and thus $\Gamma_0 = 0$) can therefore have a finite Γ_{BDA} if the Green tensor features strong gradients along the QD.

B. Decay rate of dipole-forbidden transitions

Before going on, we want to elucidate the meaning of the term *dipole-forbidden transitions* in this work. In the theory of semiconductors, the terms *dipole-allowed/forbidden* transitions is usually referred to the matrix element between the Bloch parts of the electron and hole wave functions [16]. In the framework of semiconductor QDs, excitons with a nonzero (zero) value of the Bloch matrix element are usually called bright (dark) excitons. The dark excitons are characterized by much longer lifetimes, since a spin-flip process is required before they can recombine radiatively. In this work, we still assume that the dipole approximation is valid at the level of the unit cell, and therefore the selection rules at the level of the Bloch matrix element are unaltered. However, as explained above, a secondary selection rule appears at the level of the envelope function overlap, which can be affected by the non-negligible variation of the electric field. The phenomena discussed in this paper are explicitly referred to these effects, i.e., a transition is called *forbidden* if the value of the envelope function overlap would dictate a null radiative decay rate.

Despite its general validity, Eq. (3) is difficult to handle, for two reasons. First, the structure of the six-dimensional integral makes it difficult to recognize the distinct roles of the emitter and the vacuum electromagnetic field in the decay rate. Differently from the ordinary formula [Eq. (4)], an enhancement of the LDOS in a certain point of the QD does not necessarily lead to an increase of Γ_{BDA}, since destructive interference terms can appear in Eq. (3). Second, using Eq. (3) requires very long computational time since the Green tensor must be known over the entire QD, and after that, the six-dimensional integral must be calculated with numerical techniques.

In order to overcome these problems and also to gain more insight into the physics of the dipole-forbidden (DF) transitions, we derive here a simplified version of Eq. (3). A DF transition is defined by the requirement that $\Gamma_0 = 0$. From Eq. (4), this definition implies that the quantity

$$\mu \equiv \int d^3\mathbf{r}\ \chi(\mathbf{r},\mathbf{r}) \tag{5}$$

is zero. This quantity is the term related to the envelope function in the transition dipole moment (see Appendix A).

The Green tensor can be expanded in a Taylor series up to the second-order terms,

$$G(\mathbf{r},\mathbf{r}') \simeq G(\mathbf{r_0},\mathbf{r_0}) + \nabla_{\mathbf{r}} G|_{(\mathbf{r}_0,\mathbf{r}_0)} \cdot (\mathbf{r}-\mathbf{r}_0) + \nabla_{\mathbf{r}'} G|_{(\mathbf{r}_0,\mathbf{r}_0)} \cdot (\mathbf{r}'-\mathbf{r}_0) + \tfrac{1}{2}\xi^T H[G]|_{(\mathbf{r}_0,\mathbf{r}_0)}\xi, \tag{6}$$

where $\mathbf{r_0}$ is the center of the QD, $\nabla_{\mathbf{r}}$ indicates the gradient with respect to the first spatial variable $\mathbf{r}$ (and similarly for $\nabla_{\mathbf{r}'}$), $H[G]|_{(\mathbf{r}_0,\mathbf{r}_0)}$ is the 6×6 Hessian matrix of the function G, and ξ is a 6-dimensional vector defined as $\xi = (\mathbf{r}-\mathbf{r}_0, \mathbf{r}'-\mathbf{r}_0)$. When this expansion is inserted in Eq. (3), the following approximate expression for Γ_{BDA} is obtained (the complete derivation is given in Appendix C):

$$\Gamma_{\mathrm{BDA}} = \frac{2e^2}{\hbar\epsilon_0 m_0^2 c^2}|\mathbf{p}_{\mathrm{cv}}|^2\Big[|\mu|^2\cdot\mathcal{G}(\mathbf{r_0},\mathbf{r_0}) + 2\mathrm{Re}[\mu^*\mathbf{\Lambda}]\cdot\nabla_{\mathbf{r}}\mathcal{G}|_{(\mathbf{r}_0,\mathbf{r}_0)} + \sum_{i,j=1}^{3}\Lambda_i\Lambda_j^*\partial_{r_i}\partial_{r_j'}\mathcal{G}|_{(\mathbf{r}_0,\mathbf{r}_0)} + \sum_{i,j=1}^{3}\mathrm{Re}[\mu^*\Omega_{ij}]\partial_{r_i}\partial_{r_j}\mathcal{G}|_{(\mathbf{r}_0,\mathbf{r}_0)}\Big]. \tag{7}$$

For the simplicity of notation, we defined the quantity $\mathcal{G}(\mathbf{r},\mathbf{r}') \equiv \mathrm{Im}[G_{pp}(\mathbf{r},\mathbf{r}')]$. We also introduced the quantities

$$\Lambda_i \equiv \int d^3\mathbf{r}\ (r_i - r_{i0})\chi(\mathbf{r},\mathbf{r}), \tag{8a}$$

$$\Omega_{ij} \equiv \int d^3\mathbf{r}\ (r_i - r_{i0})\ (r_j - r_{j0})\chi(\mathbf{r},\mathbf{r}). \tag{8b}$$

Λ_i is the term related to the envelope function in the magnetic-dipole and electric-quadrupole moments. Similarly, Ω_{ij} contains the higher-order terms in the multipolar expansion (see Appendix A). It is worth nothing that a similar result has been recently used [17] to study the multipolar and mesoscopic effects on the dipole-allowed (DA) transitions of semiconductor QDs. In that case only, the first two terms of the expansion were considered, since the other ones are much smaller for a DA transition. In the case of a DF transition, the first two terms and the last one disappear since $\mu = 0$, and the first nonzero term is

$$\Gamma_{\mathrm{BDA}}^{\mathrm{DF}} = \frac{2e^2}{\hbar\epsilon_0 m_0^2 c^2}|\mathbf{p}_{\mathrm{cv}}|^2\sum_{i,j=1}^{3}\Lambda_i\Lambda_j^*\ \partial_{r_i}\partial_{r_j'}\mathcal{G}|_{(\mathbf{r}_0,\mathbf{r}_0)}. \tag{9}$$

It is interesting to note that the decay rate is given by a sum of products between a field-related quantity, the mixed second derivatives of the Green tensor, and an exciton-related quantity, the vector $\mathbf{\Lambda}$. We thus obtained a simple multiplicative rule which gives clear indications on how the emitter and the vacuum field contribute to the decay rate of a DF transition. Neglecting Coulomb interactions, $\mathbf{\Lambda} = \int d^3\mathbf{r}(\mathbf{r}-\mathbf{r}_0)\chi_e(\mathbf{r})\chi_h(\mathbf{r})$, which is proportional to the matrix element of the dipole moment calculated between the envelope functions. We note that this quantity is already known in the theory of semiconductors nanostructures and it is used, for example, to calculate the selection rules for the intraband transitions of a quantum dot or a quantum well [13].

For what concerns the emitter, the figures of merit that can increase the decay rate are the quantities Λ_i. From their definition, it is clear that they can be enhanced by increasing the overall size of the QD. The enhancement of the spontaneous emission rate as the QD size increases must not be confused with the so-called giant-oscillator-strength (giant-OS) effect [18]. The giant-OS effect arises in large

QDs when the Coulomb attraction has a non-negligible effect (the so-called *weak confinement regime*) and the OS of the optically active states becomes proportional to the volume of the exciton [19]. The size dependence of the decay rate of the DF transitions is not related to the Coulomb interaction, but to the presence of the spatial coordinate in Eq. (8a). This, in the strong coupling regime, makes the quantities Λ_i scale with the QD dimensions. However, when the size of the QD becomes comparable or bigger than the exciton Bohr radius (i.e., the weak coupling regime), these effects are expected to be reduced.

Moreover, the spatial distribution of the envelope function will also affect the direction of the vector $\mathbf{\Lambda}$, which couples to the second derivatives of the Green tensor in Eq. (9). Therefore, for a fixed electromagnetic field, the decay rate has its maximum value when the vector $\mathbf{\Lambda}$ is parallel to the direction of maximum variation of the field.

The figure of merit of the electromagnetic field is related to the gradient of the field, through the mixed second derivatives of the Green tensor. For a QD embedded in a bulk material, the Green tensor can be computed analytically, and a direct calculation gives

$$\partial_{r_i}\partial_{r'_j}\mathcal{G}|_{(\mathbf{r}_0,\mathbf{r}_0)} = \delta_{ij}(2-\delta_{ip})\frac{k^3}{30\pi}, \tag{10}$$

where p is the diagonal component of the Green tensor which has been considered above (and which corresponds to the direction of the Bloch vector $\mathbf{p}_{\mathrm{cv}}$), and k is the optical wave vector in the material. By assuming that $\mathbf{\Lambda} = (\Lambda_x,0,0)$ the bulk decay rate becomes

$$\Gamma_0^{\mathrm{DF}} \propto |\Lambda_x|^2\partial_x\partial_{x'}\mathcal{G}|_{(\mathbf{r}_0,\mathbf{r}_0)} = |\Lambda_x|^2\frac{k^3}{30\pi} \tag{11}$$

and the ratio between the decay rate of a DF transition and a DA one is given by

$$\frac{\Gamma_0^{\mathrm{DF}}}{\Gamma_0^{DA}} = \frac{|\Lambda_x|^2}{|\mu|^2}\frac{k^2}{5}, \tag{12}$$

where μ is the envelope function overlap [Eq. (5)] for the DA transition, and we used the result $\mathcal{G}(\mathbf{r}_0,\mathbf{r}_0) = \frac{k}{6\pi}$ valid for homogeneous media [14].

In our derivation, we assumed that the Bloch vector $\mathbf{p}_{\mathrm{cv}}$ is constant over the volume of the emitter. This corresponds to an assumption that the Bloch functions are equal for each lattice site and they are not influenced by the strain induced by the interfaces. In a recent paper [20], it has been suggested that, for the optically active transitions, these lattice inhomogeneities (rather than the envelope-function dipole-moment) cause the main effects beyond the dipole approximation. In Appendix B, we discuss the influence of these effects on the decay rate of the DF transitions and we show that, for this case, they constitute a higher-order correction with respect to the term related to the envelope function.

A common issue in the observation of transitions involving excited states is the competition between the radiative decay and the phonon-assisted intraband relaxation [21]. Indeed, at low excitation levels and low temperatures, carriers quickly relax to the lowest available states and transitions from higher-energy states are not observed. This phenomenon, which also affects the higher-energy DA transitions, is not related with the calculation of the decay rate, but rather with the probability that a certain state is occupied. In practice, transitions from higher energy states (therefore potentially also those corresponding to DF transitions) are easily observed experimentally by increasing the excitation level and/or the temperature, in order to ensure that the corresponding states are populated. In this work, we therefore focus our attention on the calculation of radiative decay rate and we ignore the effects due to the occupation probability.

III. SPONTANEOUS EMISSION FROM DIPOLE-FORBIDDEN TRANSITIONS IN REALISTIC NANOSTRUCTURES

In this section, we illustrate some applications of the formalism developed for the DF transitions. In Sec. III A, we describe a simple model for a semiconductor QD—an InAs cylinder embedded in a GaAs matrix. In the following sections, we investigate the decay rate of the DF transitions of this QD when it is placed in two different kinds of structures—an L3 photonic crystal cavity and a plasmonic antenna. In both cases, a high enhancement of the DF transition decay rate is obtained. However, as explained in Sec. III D, these enhancements have different physical origins.

A. The disk-shaped QD with infinite barrier

A cylindrical InAs QD with radius $R = 10$ nm and height $L = 10$ nm embedded in a GaAs matrix is considered as a model for our calculations. We notice that, while the value assumed for the height is larger than the average values of 3–5 nm normally measured for semiconductor InAs/GaAs QDs [22], higher values of the QD height, consistent with our assumption, have been reported for structures emitting in the near infrared [23].

The axis of the cylinder is along the z direction. An infinite potential barrier is assumed and the Coulomb interaction is neglected because of the small dimensions of the QD. Although this simplified model is far from a realistic description of the QD (in which the strain and the real potential barrier play an important role), they can still qualitatively describe the behavior of a confined exciton. Under these simplifying assumptions, the effective-mass equation can be solved analytically. The single-particle wave function is described by three quantum numbers:

$$\Psi_{n,p,m}(\mathbf{r}) \propto e^{im\phi}J_m\left(j_{mp}\frac{\rho}{R}\right)\sin\left[n\pi\left(\frac{z}{L}+\frac{1}{2}\right)\right], \tag{13a}$$

$$n = 1,2,\ldots, \quad m = 0,\pm1,\pm2,\ldots, \quad p = 1,2,\ldots, \tag{13b}$$

where (ρ,ϕ) are the polar coordinates in the plane xy, J_m is the mth-order Bessel function, and j_{mp} is the pth zero of the Bessel function J_m. The origin is chosen in the center of the cylinder. The exciton envelope function is given by the product of the electron's and hole's wave functions, and the excitonic state is thus described by six quantum numbers,

$$\chi_{n_em_ep_en_hm_hp_h}(\mathbf{r}_e,\mathbf{r}_h) = \chi^e_{n_em_ep_e}(\mathbf{r}_e)\chi^h_{n_hm_hp_h}(\mathbf{r}_h). \tag{14}$$

It is trivial to verify that the optically active states are the ones for which the electron's and hole's quantum numbers are equal, $(n_e,m_e,p_e) = (n_h,m_h,p_h)$. The envelope function overlap μ of all these transitions is equal to 1, since in this simple model, the electron and hole envelope functions are identical. The first dipole-allowed transition is the one with $(n_e,m_e,p_e,n_h,m_h,p_h) = (1,0,1,1,0,1)$. In the following, we will refer to it as the DA transition.

A DF transition is obtained when one of the quantum numbers is different. The different excitonic states feature different symmetries of the envelope functions along different directions. For the transition described by the quantum numbers (1,0,1,2,0,1), the vector $\mathbf{\Lambda}$ is oriented along the z direction and is equal to $\mathbf{\Lambda} = (0,0,0.18) \times L$, while for the DF transition (1,0,1,1,1,1) the vector lies in the xy plane and is equal to $\mathbf{\Lambda} = 0.23 \times (1,i,0) \times R$. By using Eq. (12), the ratio between the decay rates of these transitions and that of the DA one can be found to be, for an emission wavelength of $\lambda = 1300$ nm in bulk GaAs, of the order of 10^{-4}.

The linear dependence of $\mathbf{\Lambda}$ with respect to the dimensions of the QD confirms the qualitative analysis of the previous section. In the recent years, the growth of QDs with higher aspect ratio—the so-called columnar QDs—has been demonstrated [24–26]. The height of these structures can be one order of magnitude higher with respect to ordinary InAs/GaAs self-assembled QDs. Because of the quadratic dependence on the components of $\mathbf{\Lambda}$ [see Eq. (9)], the decay rate of the DF transitions is expected to be approximately 10^2 higher in these structures, making them a good candidate for the observation of the DF transitions.

B. Photonic crystal cavity

The first optical nanostructure investigated is an L3 photonic crystal cavity (PCC). The PCC is formed by a triangular pattern of air holes etched in a 320-nm-thick GaAs membrane. The lattice parameter is $a = 320$ nm and the radius hole is $r = 0.3a$. By removing three collinear holes, an L3 cavity is formed, as showed in the inset of Fig. 1(c). The fundamental mode of this single cavity has a wavelength of $\lambda_{\mathrm{PCC}} = 1287$ nm and a Q factor of 4477 (much higher Q factors can be obtained by a fine tuning of the position and the size of the holes close to the cavity) [27]. It is well-known that the in-plane electric field components of a PCC mode feature several oscillations in the plane of the membrane, while along the out-of-plane direction the variation of the field is weaker. These observations suggest to choose a DF transition for which the vector $\mathbf{\Lambda}$ lies in the plane of the cavity as, for example, the transition described by $(n_e,m_e,p_e,n_h,m_h,p_h) = (1,0,1,1,1,1)$. We, moreover, assume that both the DF and DA transitions are resonant with the fundamental mode of the cavity. Even if this is not the case for a given QD and cavity, it gives us the possibility to compare the maximum enhancements experienced by the two transitions when the cavity and/or the QD energies are tuned. As explained above, the Bloch vector $\mathbf{p}_{\mathrm{cv}}$ lies in the xy plane and therefore both the orthogonal in-plane polarizations of the electric field should be considered. For simplicity, we consider here only the case of a y-polarized exciton since the fundamental mode of the L3 cavity is mainly polarized along the y direction.

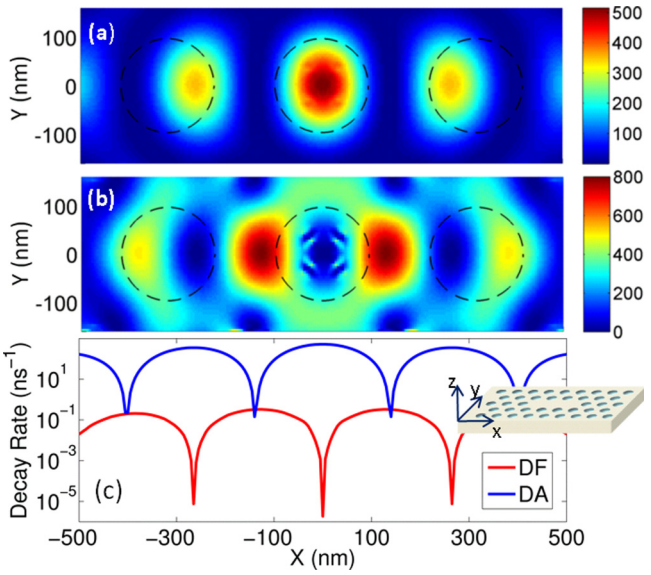

FIG. 1. (Color online) Decay rate enhancement of the DA and DF transitions as the QD is moved inside the cavity. Both the transitions are assumed to be in resonance with the PCC fundamental mode ($\lambda_{\mathrm{PCC}} = 1287$ nm) and polarized along the y direction. (a) and (b) Decay rates enhancement (as compared to their values in bulk GaAs) for the DA and DF transitions, respectively. The black dashed circles indicate the position of the holes that have been removed to create the cavity. (c) Absolute value of the decay rate for both the transitions along the line $y = 0$. The inset shows the geometry of the structure and the reference frame.

However, the calculations can be straightforwardly extended to the general case.

When dealing with a dielectric structure (i.e., a real-valued dielectric function), the Green tensor can be directly calculated from the normal modes of the electromagnetic field. The imaginary part of the Green tensor is given by [14]

$$\mathrm{Im}[G(\mathbf{r},\mathbf{r}',\omega)_{\alpha\beta}] = \frac{\pi c^2}{2\omega} \sum_k E^*_{k,\alpha}(\mathbf{r}) E_{k,\beta}(\mathbf{r}') \delta(\omega - \omega_k), \quad (15)$$

where $E_{k,\alpha}$ denotes the α component of the vacuum electric field of the kth mode. The electric field has been normalized through $\int d^3\mathbf{r}\, \epsilon_r(\mathbf{r}) \mathbf{E}^*(\mathbf{r}) \cdot \mathbf{E}(\mathbf{r}) = 1$, where $\epsilon_r(\mathbf{r})$ is the relative dielectric permittivity. Given the very small linewidth of a PCC resonance, we can safely assume that only one mode will contribute for each frequency (the leaky modes of the PCC are neglected). For realistic cavities, the delta function can be replaced by a Lorentzian function, and at resonance ($\omega = \omega_k$), we obtain

$$\mathrm{Im}[G(\mathbf{r},\mathbf{r}',\omega)_{\alpha\beta}] = Q \frac{c^2}{\omega^2} E^*_{\alpha}(\mathbf{r}) E_{\beta}(\mathbf{r}'), \quad (16)$$

where Q is the Q factor of the cavity.

In our calculations, the QD is placed in the center of the GaAs slab and moved in the xy plane inside the cavity. The electric field of the fundamental mode is calculated numerically with a commercial FDTD software [28] by exciting the structure with a dipolar source and recording the resonant field with a temporal filter. For the GaAs, we assume a refractive index of $n_{\mathrm{GaAs}} = 3.40$, while the value of $|\mathbf{p}_{\mathrm{cv}}|^2$ for

InAs is available in literature [29]. The DA and DF decay rates are calculated by using the ordinary dipole approximation and our formalism, respectively. The calculation shows that the decay rate of the DF transition [Fig. 1(b)] can be enhanced by a factor up to 800 with respect to its value in bulk GaAs. The enhancement experienced by the DA transition is of the same order of magnitude [Fig. 1(a)], although the positions of the maxima are different.

Figure 1(c) shows an interesting phenomenon predicted by our theory: intuitively, one would expect that the strongest deviations from the dipole approximation theory would appear where the square modulus of the electric field (and thus the LDOS) has its maximum variation. Therefore the decay rate of the DF transition (red curve) should have its maxima in correspondence of the points of maximum variation of the DA transition decay rate (blue curve). Instead, an inspection of the data shows that these points do not coincide and are separated by about 70 nm. The reason for this is that decay rate of the DF transitions is not directly proportional to the derivative of the electric field $|E|^2$, but is related in a more complex way to the Green tensor, as shown by our formula.

C. Plasmonic dimer antenna

The second structure investigated is a plasmonic dimer antenna. Before going on, we note that the theory developed by Stobbe *et al.* (from which the formalism presented here is derived) is not rigorously valid for a plasmonic structure. Indeed, the derivation of Eq. (3) is based on the possibility of expressing the Green tensor through the normal modes of the electromagnetic field (see Appendix C of Ref. [12]). For a plasmonic structure, the electric field is not the solution of a Hermitian problem, because of the complex-valued dielectric function. Any derivation based on the normal modes is, therefore, mathematically not well defined. This topic has been subject of intensive theoretical research in the last years [30–32]. Recently, it has been shown how the Green tensor can be expressed through the quasinormal modes of the system once they are properly renormalized [33]. With the aid of these new theoretical tools it should be possible to extend the derivation of Eq. (3) to the plasmonic case, but a formal demonstration is beyond the scope of this paper. In the following, we will assume, similarly to a recent work [17] about the spontaneous decay rate of QDs interacting with a metallic structure, that the concept of normal modes [and therefore also Eq. (3)] can be applied also to a structure with a complex dielectric permittivity.

The plasmonic structure that we consider consists of two gold nanorods placed on a GaAs substrate and separated by a gap of 30 nm. Each antenna has in-plane dimensions of 250 nm $\times$ 50 nm and is 30-nm thick. This structure supports a localized plasmonic mode at a wavelength of $\lambda_{\rm pl} = 1330$ nm, as revealed by a calculation of the power emitted by a dipole placed nearby [Fig. 2(a)]. As mentioned before, for self-assembled semiconductor QDs, the Bloch vector $\mathbf{p}_{\rm cv}$ lies in the growth plane. We assume for simplicity that the exciton can interact only with the x component of the plasmonic field, which is depicted in Fig. 2(b) along a vertical plane in the middle of the structure. The contribution from the y-polarized exciton is negligible if the QD is placed in the gap between the antenna, since here the electric field is mainly x polarized. Below the gap, a strong gradient of the field along the z direction is visible. This suggests considering a DF transition for which $\mathbf{\Lambda}$ is oriented along the z axis, as the one described by $(n_e,m_e,p_e,n_h,m_h,p_h) = (1,0,1,2,0,1)$.

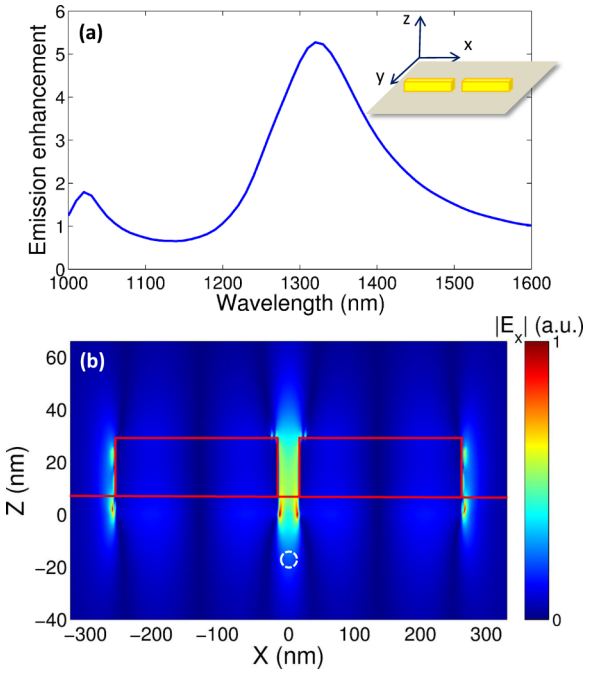

FIG. 2. (Color online) Plasmonic structure investigated. (a) Resonance spectrum of the structure obtained by calculating the enhancement of the power emitted by a dipole (with respect to the power emitted in bulk GaAs) placed nearby. The inset shows the geometry. (b) Absolute value of the x component of the electric field along the middle of the structure for a wavelength of 1330 nm. The red solid lines indicate the edges of the structure. The dashed white circle indicates one of the positions in which the decay rate of the QD has been calculated.

We evaluated (Fig. 3) the decay rate of the DA and the DF transition when the QD is placed in the center of the

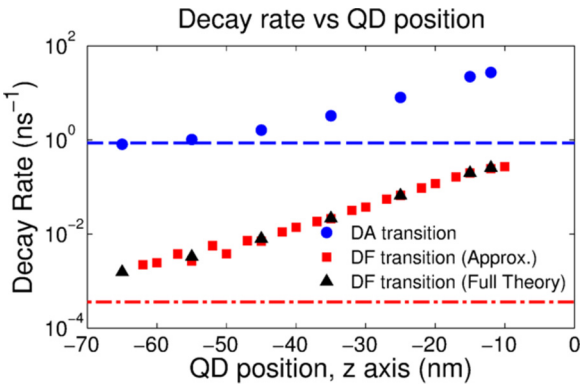

FIG. 3. (Color online) Decay rate of the DF and DA transitions as a function of the vertical distance between the QD and the plasmonic structure. The blue dashed line and the red dashed-dotted line indicate the decay rate in bulk GaAs of the DA and DF transition, respectively. The red squares are calculated with Eq. (9), while the black triangles are calculated with the full formula given by Eq. (3).

structure and moved along the z direction [see white dashed circle in Fig. 2(b)]. The two transitions are assumed to be both spectrally resonant with the plasmonic mode in order to make a fair comparison of the decay rate enhancements. The Green tensor of the structure is calculated numerically with a commercial FDTD software [28] by evaluating the response of the system to a dipolar excitation placed in different positions. The parameters used for the numerical calculation are the ones mentioned in the previous section, and the dielectric function of the gold is an interpolation of tabulated data [34]. The decay rate of the DA transition is calculated by using only the dipolar part of Eq. (7), while the decay rate of the DF transition is calculated with the formula (9). We have also evaluated, for few positions, the decay rate of the DF transition predicted by the general formula in Eq. (3) (black triangles in Fig. 3), to show that our formalism allows obtaining precise results but with a drastically reduced computational time. Specifically, the computation of the decay rate with the exact theory has required, on a personal computer, approximately five days of calculations to obtain the Green tensor in all the volume spanned by the QD in the z direction, plus several hours for the numerical calculation of the integral in Eq. (3). By using our approximated formula, it is necessary to know the derivatives of the Green tensor only in the center of the QDs, which reduces the computational time to a couple of hours (for each of the red squares in Fig. 3). After that, the computation of the decay rate through Eq. (9) requires a negligible amount of time.

Figure 3 shows the enhancement of the radiative decay rate for the DA and DF transitions as the distance between the QD and the plasmonic antenna is changed from 65 to 10 nm. We notice that, as the QD gets closer to the surface, the radiative enhancement will compete with nonradiative processes, which becomes dominant when the capping layer is reduced to few tens of nanometers [35]. The influence of the nonradiative decay rate can be reduced by passivating the surface, and capping layers as thin as 18 nm have been demonstrated [36] to be possible without a degradation of the optical properties of the QDs. We therefore consider the distance of 15 nm as a limit value for the position of the QD, below which the radiative emission will be quenched by nonradiative effects. At this position, the DA transition is enhanced by a factor of about 20 with respect to its value in bulk GaAs. This enhancement is comparable to the ones commonly calculated for this kind of structures, and it is due to the enhancement of the electric field close to the plasmonic cavity. On the other hand, the DF transition is enhanced by a factor larger than 370, which cannot be explained only as an effect of the field enhancement. This enhancement is due to the variation of the electromagnetic field along the QD, which increases the quantity $\partial_z \partial_{z'} \mathcal{G}|_{(\mathbf{r}_0,\mathbf{r}_0)}$ from its bulk value [given by Eq. (10)].

D. Comparison between the plasmonic and PCC structure

In the previous sections, we calculated the decay rate of the DF transitions for a cylindrical QD interacting with a metallic structure and a dielectric cavity. In both cases, we obtained an enhancement with respect to its bulk value of about 10^2–10^3. With this enhancement factor, the DF decay rate should be comparable with the bulk decay rate of a DA transition, and thus experimentally observable. However, despite the numerous experiments carried on in the last years with semiconductor QDs embedded in PCC cavities, no observation of the DF transitions has been reported. We propose here an explanation for this apparently contradictory result.

Although the DF decay rates for the plasmonic and PCC structures are of the same order of magnitude, their ratio with the (maximum) Purcell factor of the respective DA transition is very different; in the case of the plasmonic structure, the DF transition experiences a decay rate enhancement, which is almost 20 times greater than the one of the corresponding DA transition. For the PCC cavity, this ratio is about 1.5. This large difference suggests a different origin of the two enhancements.

The enhancement of the DF decay rate can be separated into two contributions; first, the decay rate is increased by the multipolar effects, which are relevant when the field cannot be assumed constant; these effects do not depend on the absolute value of the field but only on its variation. Once the decay rate is increased (from the null value that it would have in the dipole approximation to a finite value) the Purcell effect, which depends on the square of the vacuum electromagnetic field, provides a further enhancement.

For the case of a dielectric structure, this factorization can be shown analytically. The effective mode volume of the normal mode $\mathbf{E}(\mathbf{r})$ is given by

$$V = \frac{\int d^3\mathbf{r}\, \epsilon_r(\mathbf{r})\mathbf{E}^*(\mathbf{r})\cdot\mathbf{E}(\mathbf{r})}{[\epsilon_r(\mathbf{r})|\mathbf{E}(\mathbf{r})|^2]_{\mathrm{Max}}} = \frac{1}{[\epsilon_r(\mathbf{r})|\mathbf{E}(\mathbf{r})|^2]_{\mathrm{Max}}}, \quad (17)$$

where the normalization shown in Sec. III B has been used. By multiplying and dividing the right term of Eq. (16) for the mode volume, the Green tensor can be rewritten as

$$\mathrm{Im}[G(\mathbf{r},\mathbf{r}',\omega)_{\alpha\beta}] = \frac{n^3}{3\lambda_0}\frac{E^*_\alpha(\mathbf{r})E_\beta(\mathbf{r}')}{[\epsilon_r(\mathbf{r})|\mathbf{E}(\mathbf{r})|^2]_{\mathrm{Max}}} \quad (18)$$

$$\times\left[\frac{3}{4\pi^2}\left(\frac{\lambda_0}{n}\right)^3\frac{Q}{V}\right], \quad (19)$$

where λ_0 is the vacuum wavelength and n is the refractive index of the material. The well-known expression for the Purcell factor is retrieved in the second factor of the right term. The first factor, which contains the spatial dependence of the field (but does not depends on its absolute value), is responsible for the enhancement due to the multipolar effects.

The Purcell factor can be obtained by looking at the maximum enhancement of the DA transition, which is not affected by the multipolar effects. For the PCC structure, this value is about 500 [Fig. 1(c)]. This means that the contribution of the multipolar effects to the DF decay rate enhancement is about 1.5. The enhancement of the DF transitions is, therefore, almost entirely due to the Purcell effect. However, despite the high values of the Purcell factor calculated for a PCC, the experimentally measured decay rate enhancements are systematically much lower. The current record for the Purcell factor in a PCC slab containing QDs is about 10 [37]. The origin of this huge mismatch between the theoretical and experimental values is usually attributed to the poor spatial matching between the QD and the cavity field, but this has not yet been proved. If we assume a realistic value for the Purcell factor, it is clear how the expected enhancement of the DF

transitions is drastically reduced with respect to the theoretical values calculated in Fig. 1(c).

On the other hand, for the plasmonic structure, the contributions from the Purcell effect and from the field inhomogeneities are of the same order of magnitude. Moreover, the experimental values of the Purcell factor for this kind of metallic structures are usually not far from the calculated ones [36]. We conclude therefore that a metallic structure constitutes a more promising candidate to experimentally observe the DF transitions of a QD.

IV. CONCLUSIONS

We have theoretically investigated the multipolar effects on the DF transitions of a semiconductor QD. We obtained a simplified expression for the decay rate of these transitions that allows us to identify the figures of merit for its enhancement. The figure of merit of the emitter is given by the dipole moment over the envelope functions, $\mathbf{\Lambda}$, which can be increased either by increasing the overall dimension of the QD or by engineering the exciton envelope functions, in order to increase their asymmetry. Moreover, the direction of this vector must coincide with the direction along which the vacuum electric field features the maximum variation. This variation is quantified analytically by the mixed second derivatives of the imaginary part of the Green tensor.

We have applied our formalism to the case of a cylindrical InAs/GaAs QD interacting with two different nanocavities, a plasmonic dimer antenna and an L3 photonic crystal cavity. The decay rate of the DF transition is enhanced, in both cases, by a factor of about 10^2–10^3 with respect to its bulk value. We showed, however, that in the case of the PCC the decay rate enhancement is mainly due to the Purcell effect and not to the multipolar effects. This could represent a problem for the experimental observation of these transitions, since the measured values of the Purcell factor in PCC structures are usually much lower than the calculated ones. On the other hand, for the plasmonic structure, the contribution of the multipolar effects is higher, because of the high gradient of the field close to the metallic surface. We therefore conclude that this kind of structure represents a more promising choice to observe experimentally the DF transitions of a QD.

ACKNOWLEDGMENTS

The authors acknowledge F. Koenderink for stimulating discussions and S. Stobbe and P. Tighineanu for reading the manuscript and providing critical comments. This work is part of the research programme of the Foundation for Fundamental Research on Matter (FOM), which is financially supported by the Netherlands Organisation for Scientific Research (NWO).

APPENDIX A: MULTIPOLAR MOMENTS

In the main text, we introduced the quantities μ, Λ_i, and Ω_{ij} to describe the multipolar effects on the dipole-forbidden transitions of a semiconductor QD. Here, we want to show the link between these quantities and the ones that are usually introduced in the multipolar expansion of the light-matter interaction. When describing the interaction of a general quantum system (such as an atom or a molecule) with light, the decay rate can be expressed as a sum of infinite terms [38]; the first three terms contain the quantities

$$\widetilde{\mu}_i = \langle g|\, \hat{p}_i\, |e\rangle, \tag{A1a}$$

$$\widetilde{\Lambda}_{ij} = \langle g|\, \hat{r}_i \hat{p}_j\, |e\rangle, \tag{A1b}$$

$$\widetilde{\Omega}_{ijk} = \langle g|\, \hat{r}_i \hat{r}_j \hat{p}_k\, |e\rangle, \tag{A1c}$$

where $\hat{r}_i$ and $\hat{p}_i$ are the components of the position and momentum operators of the system along the ith direction, and $|g\rangle$ and $|e\rangle$ are the ground and the excited states of the quantum system. For an exciton in a low-energy state of a semiconductor QD, the electron wave function can usually be approximated by the product $|e\rangle = |u\rangle\,|\chi\rangle$ of a periodic Bloch function, which oscillates on the length scale of the lattice parameter, and a slowly varying envelope function. A good approximation is thus to assume that the envelope function does not vary along a unit cell. This allows us to rewrite the dipole moment $\widetilde{\mu}_i$ as

$$\widetilde{\mu}_i \simeq \langle u_g|\, \hat{p}_i\, |u_e\rangle \cdot \langle \chi_g|\chi_e\rangle = (\mathbf{p}_{\mathrm{cv}})_i \mu, \tag{A2}$$

where the definitions introduced in the main text have been used. The derivation of Eq. (A2) can be found in standard textbooks [13], and a similar approach (assuming that also the derivatives of the envelope function do not vary along a unit cell) can be used to show that

$$\begin{aligned}\widetilde{\Lambda}_{ij} \simeq\ & \langle u_g|\, \hat{p}_j\, |u_e\rangle\, \langle \chi_g|\, \hat{r}_i\, |\chi_e\rangle + \langle u_g|\, \hat{p}_j \hat{r}_i\, |u_e\rangle\, \langle \chi_g|\chi_e\rangle \\ & + \langle u_g|u_e\rangle\, \langle \chi_g|\, \hat{p}_j \hat{r}_i\, |\chi_e\rangle + \langle u_g|\, \hat{r}_i\, |u_e\rangle\, \langle \chi_g|\, \hat{p}_j\, |\chi_e\rangle\,.\end{aligned} \tag{A3}$$

As explained in the main text, for semiconductor QDs, the periodic Bloch function u_g is the one of the heavy hole band, which has the symmetry of the p_x or p_y orbital [13]. The electron Bloch function u_e is instead spherically symmetric. It is therefore trivial to verify that the second and third terms vanish for any choice of i and j. The fourth term scales with the size of the unit cell, and is thus negligible compared to the first one, which scales with the size of the QD. We conclude therefore that $\widetilde{\Lambda}_{ij} \simeq (\mathbf{p}_{\mathrm{cv}})_j\, \langle \chi_g|\, \hat{r}_i\, |\chi_e\rangle = (\mathbf{p}_{\mathrm{cv}})_j \Lambda_i$. The tensor $\widetilde{\Lambda_{ij}}$, which in the general theory of the light-matter interaction describes the electric-quadrupole and magnetic-dipole moments, is here related to the dipole moment over the envelope functions and to the microscopic dipole moment $\mathbf{p}_{\mathrm{cv}}$. Similar considerations can be done for the electric-octupole and magnetic-quadrupole moments $\widetilde{\Omega}_{ij}$.

APPENDIX B: QUANTITATIVE ESTIMATION OF THE INFLUENCE OF LATTICE INHOMOGENEITIES

In our derivation, we neglected the effects of the variation of the lattice constant and/or the material composition on the exciton's wave function. We assumed, in particular, that the Bloch vector $\mathbf{p}_{\mathrm{cv}} = \langle u_{c,0}|\, \hat{\mathbf{p}}\, |u_{v,0}\rangle$ lies in the plane xy (i.e., the growth plane) and that it is constant along the QD. The absence of a vertical component p_z is due to the symmetry of the heavy hole's and electron's Bloch functions in a bulk semiconductor. These assumptions lead to a simplification of the dipolar and multipolar terms, as explained in Appendix A. In particular,

once the component of the Bloch vector is fixed and assumed constant (e.g., $\mathbf{p}_{cv} = p_x \hat{\mathbf{e}}_x$), the dipolar and multipolar terms become

$$\begin{aligned} \widetilde{\mu}_x &= \langle \chi_h | \chi_e \rangle \;\; p_x = \mu \;\; p_x, \\ \widetilde{\Lambda}_{ix} &= \langle \chi_h | \hat{r}_i \, | \chi_e \rangle \;\; p_x = \Lambda_i \;\; p_x, \end{aligned} \tag{B1}$$

where μ and Λ_i are defined in the main text.

When considering a heterostructure where the lattice constant and/or composition are not uniform, as commonly encountered in self-assembled QDs, both assumptions are in principle not correct. The in-plane component of the Bloch vector p_x can vary along the QD, and the vertical component p_z can have a local nonzero value in correspondence of the strained unit cells. In a recent paper [20] by Tighineanu *et al.*, it has been suggested that, for the optically active transitions, these lattice inhomogeneities (rather than the envelope-function dipole-moment) cause the main effects beyond the dipole approximation. The reason is that for these transitions the equal parity of the envelope functions makes the value of Λ_i [as calculated with Eq. (8a)] small compared to the value of μ, and it cannot explain the high value of Λ/μ found experimentally [7]. Nevertheless, for the DF transitions, the different parity of the envelope function leads to smaller values of μ and larger values of Λ, which suggests that the contribution from the envelope functions to the multipolar moment Λ can overcome the one due to the strain, as assumed in the derivation of Eq. (9). In this appendix, we justify this assumption by providing a quantitative estimation of these effects for two different cases.

First, we assume that the in-plane component of the Bloch vector has a slow linear variation across the QD height. We consider only the component p_x for the sake of clarity. The calculation of $\widetilde{\mu}_x$ must be generalized to take into account the position dependence of p_x, giving

$$\widetilde{\mu}_x = \sum_N \chi_h^*(\mathbf{R}_N)\chi_e(\mathbf{R}_N)p_x(\mathbf{R}_N), \tag{B2}$$

where the sum is over all the unit cells and $\mathbf{R}_N$ is the position of the Nth cell. In this case, $\widetilde{\mu}_x$ can be different from zero even if $\langle \chi_h | \chi_e \rangle = 0$. Therefore the first term of the Taylor expansion in Eq. (7) (from now on called Γ_0) may not be negligible compared to the third term (from now on called Γ_2). By assuming a linear variation of $p_x(\mathbf{R}_N)$ across the height of the QD, we can obtain a simple formula to estimate the magnitude of the two terms,

$$\frac{\Gamma_0}{\Gamma_2} = \left| \frac{\Delta p_x / p_x}{L} \right|^2 \frac{\mathrm{Im}[G_{xx}(\mathbf{r}_0, \mathbf{r}_0)]}{\partial_z \partial_z' \mathrm{Im}[G_{xx}(\mathbf{r}_0, \mathbf{r}_0)]}, \tag{B3}$$

where $\Delta p_x / p_x$ is the relative variation of p_x, with respect to its average value, across the height L of the QD. In Fig. 4(a), we show the results of this calculation for a QD with $L = 10$ nm interacting with the plasmonic structure discussed in the main text, and for different values of $\Delta p_x / p_x$. For reasonable values of $\Delta p_x / p_x < 10\%$, the contribution Γ_0 to the decay rate constitutes a negligible fraction of the total decay rate. Although a more detailed knowledge of the distribution of p_x would be necessary to make a precise estimation, this analysis provides a good indication of the order of magnitude of the effects due to the dipole moment $\widetilde{\mu}_x$ induced by lattice inhomogeneities.

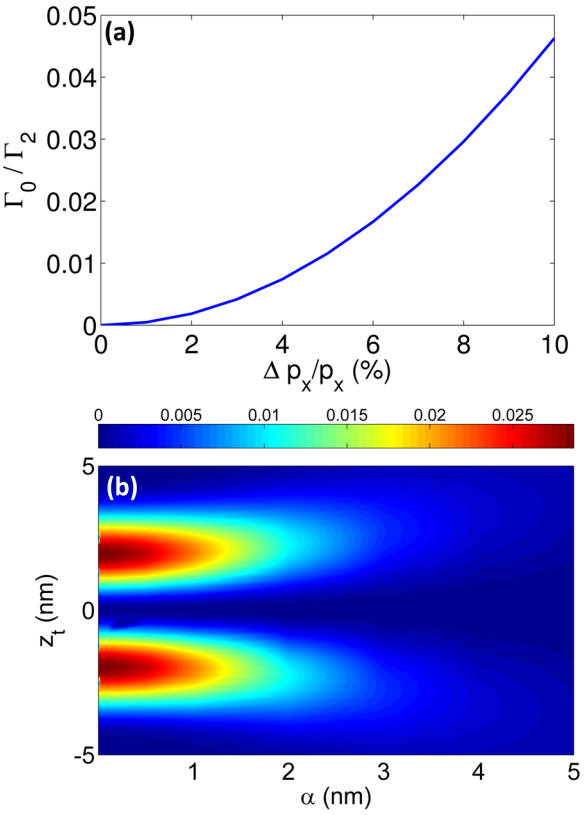

FIG. 4. (Color online) Influence of the strain on the decay rate of a DF transition. (a) Ratio between the strain-induced dipolar term of the decay rate (Γ_0) and the decay rate due to the envelope-function multipolar moment (Γ_2) as a function of the relative variation of the Bloch vector Δp_x for a QD interacting with the plasmonic structure discussed in the main text. (b) Values of $|\widetilde{\Lambda}_{xz}/\widetilde{\Lambda}_{zx}|^2$ for different values of the parameter α and for different positions of the strained layer across the QD height ($L = 10$ nm). α represents the HWHM of the normal distribution, which describes the local change of the lattice vector. For these calculations, we considered the DF transition discussed in Sec. III C.

A second case to take into account is a possible nonzero value of the z component of the Bloch vector in correspondence to high-strained unit cells. This is indeed the case studied in the work mentioned above [20]. For the optically active transition discussed there, the only nonzero elements of the multipolar tensor $\widetilde{\Lambda}$ are $\widetilde{\Lambda}_{zx}$ and $\widetilde{\Lambda}_{xz}$. The first one is very small for the transition considered by the authors, because of the equal parity of the envelope functions of a DA transition along the z direction. The second term, which would be zero in absence of strain since $p_z = 0$, gives in fact the main contribution to the multipolar decay rate when a strained layer is assumed to exist in the QD [20]. We notice that the term $\widetilde{\Lambda}_{zx}$ corresponds to the effects discussed in this paper for the DF transitions, i.e., a constant in-plane Bloch vector p_x multiplied by a dominant contribution from the envelope functions integral. One could therefore wonder if also for a DF transition the term $\widetilde{\Lambda}_{xz}$ can become important in presence of strain. We define the

following two contributions to the multipolar decay rate:

$$\Gamma_2^{\text{Inhom}} \propto |\widetilde{\Lambda}_{xz}|^2 \partial_x \partial'_x \text{Im}[G_{zz}(\mathbf{r}_0,\mathbf{r}_0)],$$
$$\Gamma_2^{\text{Env}} \propto |\widetilde{\Lambda}_{zx}|^2 \partial_z \partial'_z \text{Im}[G_{xx}(\mathbf{r}_0,\mathbf{r}_0)]. \quad \text{(B4)}$$

We notice that the derivatives and the components of the Green tensor are different, since the different elements of the tensor $\widetilde{\Lambda}$ couple to different components (and derivatives) of the electromagnetic field. To make a fair comparison between the two terms, we ignore the influence of the electromagnetic field, since it can always be engineered in such a way to make one of the two effects dominant. We therefore consider the ratio $|\widetilde{\Lambda}_{xz}/\widetilde{\Lambda}_{zx}|^2$ as a quantitative estimation of the influence of the two effects. We then need to generalize the calculation of the tensor $\widetilde{\Lambda}$ to take into account the position dependence of the Bloch vector,

$$\widetilde{\Lambda}_{ij} = \sum_N \chi_h^*(\mathbf{R}_N)\chi_e(\mathbf{R}_N)R_{N,i} \quad p_j(\mathbf{R}_N), \quad \text{(B5)}$$

where $R_{N,i}$ denotes the ith coordinate of the Nth unit cell. To calculate the components of the Bloch vector, we need the functional expression of the electron's and hole's Bloch function. In order to compare our results with the ones showed in the work of Tighineanu *et al.* [20], we assume here the same ansatz on the Bloch functions [Eq. (2) of Ref. [20]]: the conduction and valence Bloch functions are expanded in a sum of sinusoidal functions with a z-dependent period $a(z)$. A simple calculation leads to

$$\frac{\widetilde{\Lambda}_{xz}}{\widetilde{\Lambda}_{zx}} = \frac{\langle\chi_h|x^2K'(z)|\chi_e\rangle}{\langle\chi_h|zK(z)|\chi_e\rangle}, \quad \text{(B6)}$$

where $K'(z)$ denotes the derivative of lattice wave vector $K(z) = 2\pi/a(z)$ along the z direction. In their work, the authors assumed $K'(z) = \Delta K\delta(z - z_t)$, i.e., the periodicity of the unit cells is broken only along an infinitely thin layer, localized at the height z_t in the QD and normal to the growth direction. We consider a more general case where the periodicity change is described by $K'(z) = \Delta K\delta_\alpha(z - z_t)$, where $\delta_\alpha(z - z_t) = (\alpha\sqrt{\pi})^{-1}e^{-\frac{(z-z_t)^2}{\alpha^2}}$ is a normal distribution which tends to the delta function when the parameter α approaches zero. This leads to

$$\frac{\widetilde{\Lambda}_{xz}}{\widetilde{\Lambda}_{zx}} = \frac{\Delta a}{a}\frac{\langle\chi_h|x^2\delta_\alpha(z - z_t)|\chi_e\rangle}{\langle\chi_h|z|\chi_e\rangle}, \quad \text{(B7)}$$

where $\Delta a/a$ is the relative change of the lattice constant along the strained layer at z_t. According to the available experimental data [39], we assume $\Delta a/a = 0.18$. In Fig. 4(b), we report the value of the ratio $|\widetilde{\Lambda}_{xz}/\widetilde{\Lambda}_{zx}|^2$ for different values of the parameter α and for different positions of the strained layer across the QD height ($L = 10$ nm). Even for $\alpha \simeq 0$ (i.e., a delta-function-dependent lattice vector variation) and for an optimal position along the QD, the effects due to the inhomogeneities constitutes less than 3% of the envelope-functions contribution.

In this appendix, we provided an explicit calculation of the lattice inhomogeneities effects for two different cases. Of course, other possible cases should be considered, and each of them would require a dedicated analysis [e.g., in the second term of Eq. (9) the simultaneous effect of a slow-varying p_x and a local nonzero value of p_z can be considered in evaluating the product $\mu^* \cdot \mathbf{\Lambda}$]. However, we believe that the results shown in this appendix constitute a valid quantitative estimation of the order of magnitude of these effects, and the formulas provided can be easily modified to take in account other cases of interest.

APPENDIX C: DERIVATION OF THE DECAY RATE FOR THE DF TRANSITIONS

We derive here the formula for the decay rate of the DF transition [Eq. (7)]. When the Taylor expansion of the Green tensor [Eq. (6)] is inserted in Eq. (3), the following expansion for the decay rate is obtained:

$$\begin{aligned}\Gamma_{\text{BDA}} \propto\ & \mathcal{G}(\mathbf{r_0},\mathbf{r_0})\left|\int d^3\mathbf{r}\ \chi(\mathbf{r},\mathbf{r})\right|^2 \\ & + \nabla_{\mathbf{r}}\mathcal{G}|_{(\mathbf{r}_0,\mathbf{r}_0)}\int d^3\mathbf{r}\chi(\mathbf{r},\mathbf{r})\ (\mathbf{r}-\mathbf{r}_0)\int d^3\mathbf{r}'\ \chi(\mathbf{r}',\mathbf{r}') \\ & + \nabla_{\mathbf{r}'}\mathcal{G}|_{(\mathbf{r}_0,\mathbf{r}_0)}\int d^3\mathbf{r}\chi(\mathbf{r},\mathbf{r})\int d^3\mathbf{r}'\chi^*(\mathbf{r}',\mathbf{r}')\ (\mathbf{r}'-\mathbf{r}_0) \\ & + \frac{1}{2}\int d^3\mathbf{r}\int d^3\mathbf{r}'\chi(\mathbf{r},\mathbf{r})\chi^*(\mathbf{r}',\mathbf{r}')\ \xi^T H[\mathcal{G}]|_{(\mathbf{r}_0,\mathbf{r}_0)}\xi, \end{aligned} \quad \text{(C1)}$$

where all the notations have been already defined in the main text. In the first three terms, the quantities μ and $\mathbf{\Lambda}$ can be easily recognized. Moreover, because of the reciprocity of the Green tensor, the equality $\nabla_{\mathbf{r}}\mathcal{G}|_{(\mathbf{r}_0,\mathbf{r}_0)} = \nabla_{\mathbf{r}'}\mathcal{G}|_{(\mathbf{r}_0,\mathbf{r}_0)}$ holds, and thus the second and third terms can be added together, resulting in $2\text{Re}(\mu^*\mathbf{\Lambda}) \cdot \nabla_{\mathbf{r}}\mathcal{G}|_{(\mathbf{r}_0,\mathbf{r}_0)}$. Therefore we just need to show that the last term of Eq. (C1) is equal to the last two terms of Eq. (7). In order to do this, it is convenient to first write explicitly the matrix product

$$\begin{aligned}\xi^T \cdot H[\mathcal{G}] \cdot \xi =\ & \sum_{i,j=1}^{3} r_i r_j \partial_{r_i}\partial_{r_j}\mathcal{G} + \sum_{i,j=1}^{3} r_i r'_j \partial_{r_i}\partial_{r'_j}\mathcal{G} \\ & + \sum_{i,j=1}^{3} r'_i r_j \partial_{r'_i}\partial_{r_j}\mathcal{G} + \sum_{i,j=1}^{3} r'_i r'_j \partial_{r'_i}\partial_{r'_j}\mathcal{G}. \end{aligned} \quad \text{(C2)}$$

Here and in what follows, we assume that $\mathbf{r}_0 = 0$, and we omit it in the derivatives for the simplicity of notation. When the first term is inserted in the integral of the last term of Eq. (C1), we obtain

$$\begin{aligned}& \frac{1}{2}\int d^3\mathbf{r}\int d^3\mathbf{r}'\chi(\mathbf{r},\mathbf{r})\chi^*(\mathbf{r}',\mathbf{r}')\ \sum_{i,j=1}^{3} r_i r_j \partial_{r_i}\partial_{r_j}\mathcal{G} \\ & = \frac{1}{2}\sum_{i,j=1}^{3}\partial_{r_i}\partial_{r_j}\mathcal{G}\int d^3\mathbf{r}\ \chi(\mathbf{r},\mathbf{r}) r_i r_j \int d^3\mathbf{r}'\chi^*(\mathbf{r}',\mathbf{r}') \\ & = \frac{1}{2}\sum_{i,j=1}^{3}\partial_{r_i}\partial_{r_j}\mathcal{G}\ \Omega_{ij}\ \mu^*. \end{aligned} \quad \text{(C3)}$$

An analogous result can be obtained for the fourth term of Eq. (C2), and by exploiting again the reciprocity of the Green tensor, the two terms can be added together, resulting in $\sum_{i,j=1}^{3}\text{Re}[\mu^*\Omega_{ij}]\partial_{r_i}\partial_{r_j}\mathcal{G}$, which is the third term of Eq. (7).

Finally, by inserting the second term of Eq. (C2) in the integral in the last term of Eq. (C1), we obtain

$$\frac{1}{2}\int d^3\mathbf{r}\int d^3\mathbf{r}'\chi(\mathbf{r},\mathbf{r})\chi^*(\mathbf{r}',\mathbf{r}')\sum_{i,j=1}^{3} r_i r'_j \partial_{r_i}\partial_{r'_j}\mathcal{G} = \frac{1}{2}\sum_{i,j=1}^{3}\partial_{r_i}\partial_{r'_j}\mathcal{G}\left[\int d^3\mathbf{r}\chi(\mathbf{r},\mathbf{r})r_i\right]\left[\int d^3\mathbf{r}'\chi^*(\mathbf{r}',\mathbf{r}')r'_j\right]$$

$$= \frac{1}{2}\sum_{i,j=1}^{3}\partial_{r_i}\partial_{r'_j}\mathcal{G}\ \Lambda_i\ \Lambda_j^*. \tag{C4}$$

The contribution of the third term of Eq. (C2) can be shown to be equal, and therefore when these two terms are summed together, the last term of Eq. (7) is obtained.

[1] P. Lodahl, S. Mahmoodian, and S. Stobbe, Rev. Mod. Phys. **87**, 347 (2015).
[2] R. Trotta, E. Zallo, E. Magerl, O. G. Schmidt, and A. Rastelli, Phys. Rev. B **88**, 155312 (2013).
[3] A. Badolato, K. Hennessy, M. Atatre, J. Dreiser, E. Hu, P. M. Petroff, and A. Imamolu, Science **308**, 1158 (2005).
[4] A. J. Bennett, R. B. Patel, J. Skiba-Szymanska, C. A. Nicoll, I. Farrer, D. A. Ritchie, and A. J. Shields, Appl. Phys. Lett. **97**, 031104 (2010).
[5] M. Bayer, G. Ortner, O. Stern, A. Kuther, A. Gorbunov, A. Forchel, P. Hawrylak, S. Fafard, K. Hinzer, T. Reinecke *et al.*, Phys. Rev. B **65**, 195315 (2002).
[6] S. Strauf and F. Jahnke, Laser Photon. Rev. **5**, 607 (2011).
[7] M. L. Andersen, S. Stobbe, A. S. Sørensen, and P. Lodahl, Nat. Phys. **7**, 215 (2011).
[8] M. Sugawara, Phys. Rev. B **51**, 10743 (1995).
[9] B. Gil and A. V. Kavokin, Appl. Phys. Lett. **81**, 748 (2002).
[10] K. J. Ahn and A. Knorr, Phys. Rev. B **68**, 161307 (2003).
[11] H. Ishihara, J. Phys.: Condens. Matter **16**, R247 (2004).
[12] S. Stobbe, P. T. Kristensen, J. E. Mortensen, J. M. Hvam, J. Mørk, and P. Lodahl, Phys. Rev. B **86**, 085304 (2012).
[13] E. Rosencher and B. Vinter, *Optoelectronics* (Cambridge University Press, Cambridge, 2002).
[14] L. Novotny and B. Hecht, *Principles of Nano-Optics* (Cambridge University Press, 2006).
[15] S. Stobbe, J. Johansen, P. T. Kristensen, J. M. Hvam, and P. Lodahl, Phys. Rev. B **80**, 155307 (2009).
[16] P. Y. Yu and M. Cardona, *Fundamentals of Semiconductors* (Springer, 2005).
[17] P. Tighineanu, M. L. Andersen, A. S. Sørensen, S. Stobbe, and P. Lodahl, Phys. Rev. Lett. **113**, 043601 (2014).
[18] L. C. Andreani, G. Panzarini, and J.-M. Gérard, Phys. Rev. B **60**, 13276 (1999).
[19] E. Hanamura, Phys. Rev. B **37**, 1273 (1988).
[20] P. Tighineanu, A. S. Sørensen, S. Stobbe, and P. Lodahl, Phys. Rev. Lett. **114**, 247401 (2015).
[21] T. Grange, R. Ferreira, and G. Bastard, Phys. Rev. B **76**, 241304 (2007).
[22] J. Márquez, L. Geelhaar, and K. Jacobi, Appl. Phys. Lett. **78**, 2309 (2001).
[23] B. Alloing, C. Zinoni, L. Li, A. Fiore, and G. Patriarche, J. Appl. Phys. **101**, 024918 (2007).
[24] J. He, R. Notzel, P. Offermans, P. Koenraad, Q. Gong, G. Hamhuis, T. Eijkemans, and J. Wolter, Appl. Phys. Lett. **85**, 2771 (2004).
[25] J. He, H. Krenner, C. Pryor, J. Zhang, Y. Wu, D. Allen, C. Morris, M. Sherwin, and P. Petroff, Nano Lett. **7**, 802 (2007).
[26] L. Li, M. Mexis, P. Ridha, M. Bozkurt, G. Patriarche, P. Smowton, P. Blood, P. Koenraad, and A. Fiore, Appl. Phys. Lett. **95**, 221116 (2009).
[27] Y. Akahane, T. Asano, B.-S. Song, and S. Noda, Nature (London) **425**, 944 (2003).
[28] Lumerical solutions, inc., http://www.lumerical.com/tcad-products/fdtd/.
[29] I. Vurgaftman, J. Meyer, and L. Ram-Mohan, J. Appl. Phys **89**, 5815 (2001).
[30] A. F. Koenderink, Opti. Lett. **35**, 4208 (2010).
[31] P. T. Kristensen and S. Hughes, ACS Photon. **1**, 2 (2013).
[32] C. Sauvan, J.-P. Hugonin, I. S. Maksymov, and P. Lalanne, Phys. Rev. Lett. **110**, 237401 (2013).
[33] R.-C. Ge, P. T. Kristensen, J. Young, and S. Hughes, New J. Phys. **16**, 113048 (2014).
[34] P. B. Johnson and R. W. Christy, Phys. Rev. B **6**, 4370 (1972).
[35] C. Wang, A. Badolato, I. Wilson-Rae, P. Petroff, E. Hu, J. Urayama, and A. Imamoğlu, Appl. Phys. Lett. **85**, 3423 (2004).
[36] M. Pfeiffer, K. Lindfors, H. Zhang, B. Fenk, F. Phillipp, P. Atkinson, A. Rastelli, O. G. Schmidt, H. Giessen, and M. Lippitz, Nano Lett. **14**, 197 (2013).
[37] D. Englund, D. Fattal, E. Waks, G. Solomon, B. Zhang, T. Nakaoka, Y. Arakawa, Y. Yamamoto, and J. Vučković, Phys. Rev. Lett. **95**, 013904 (2005).
[38] S. Bernadotte, A. J. Atkins, and C. R. Jacob, J. Chem. Phys. **137**, 204106 (2012).
[39] H. Eisele, A. Lenz, R. Heitz, R. Timm, M. Dähne, Y. Temko, T. Suzuki, and K. Jacobi, J. of Appl. Phys. **104**, 124301 (2008).